Digital Applications in Archaeology and Cultural Heritage 16 (2020) e00128

Contents lists available at ScienceDirect

Digital Applications in Archaeology and Cultural Heritage

journal homepage: www.elsevier.com/locate/daach

Energy optimization of a light projection system for buildings that virtually restores artworks

D. Vázquez [a], A.A. Fernández-Balbuena [a], H. Canabal [a], C. Muro [b], D. Durmus [c], W. Davis [c], A. Benítez [d], S. Mayorga [a,*]

[a] Department of Optics, University Complutense of Madrid, Spain
[b] Restoration Department, National Museum "Centro de Arte Reina Sofía", Spain
[c] The University of Sydney School of Architecture, Design and Planning, Australia
[d] Department of Journalism and Audio-visual Communication, Carlos III University of Madrid, Spain

ARTICLE INFO

Keywords:
Illumination system buildings
Virtual restoration
Energy optimization

ABSTRACT

The need to achieve energy efficiency standards in the lighting systems of buildings makes it necessary to optimize all aspects of them. Here, the development of a light projection system that achieves this goal by studying and modifying the spectral output, compared to conventional illumination, is described. A lighting system that estimates the reflectance characteristics of artwork and emits optimized lighting can reduce light absorption. A damage-minimizing point-by-point light projection system is developed using an optimization algorithm, to improve the appearance of the surfaces of artworks whose color has faded. In this case, a simulation of an aged oil painting was made by manipulating the original photograph, which was printed and to which the proposed system was applied. The results show that, when the aged printed image is illuminated with the optimized light source, it appears indistinguishable from the non-aged oil painting.

1. Introduction

The institutions responsible for cultural heritage are obliged to conserve and exhibit the works of art in their collections. The necessary exhibition of artwork causes deterioration due to a variety external agents, including inappropriate humidity/temperature (Pavlogeorgatos, 2003) (Mueller, 2013), and optical radiation (Michalski, 2013). The former are actually well controlled in museums, damage due to these factors are not considered here. The latter, radiation, is controlled in the ultraviolet (UV) and infrared (IR) wavelength ranges with the use of cut-off filters. But the optical radiation in the visible spectrum (380 nm–780 nm) is needed to see the artwork. Radiation causes damage to the artwork through a process called photochemical action. When photons are absorbed by a pigment, the energy state of the pigment increases, and its chemical composition can change, which produces undesirable effects in paintings, such as the discoloration of the paints (Schaeffer, 2002). The incident spectral power distribution (SPD), light intensity, exposure duration, and sensitivity of the material are four important parameters of photochemical action (CIE, 2004). While exposure duration and light source intensity have straightforward effects, they are not linear (Mayorga et al., 2016).

The Berlin model proposes a damage function to quantify the effect of a light source on different types of artwork (CIE, 2004). The damage function takes irradiance (i.e., the intensity of incident radiation) and the sensitivity of five types of materials (low-grade paper, rag paper, oil paints, textiles, and water colors) into account. The calculations indicate that radiation of shorter wavelengths causes more damage than longer wavelengths (Hilbert et al., 1991; CIE, 2004). Short wavelength radiation (e.g., UV, blue light) causes more damage due to the higher energy of the photons, while radiation of longer wavelengths (e.g., IR, red light) tends to cause damage through radiating heating effects (Cuttle, 1996).

Saunders and Kirby examined the spectral reflectance functions of different pigments and the damage caused by optical radiation and found a strong relationship between the spectral reflectance function of a pigment and damage caused by optical radiation (Saunders and Kirby, 1994). For example, damage to red objects is caused by radiation absorbed in the shorter wavelengths, while blue objects deteriorate due to the light absorbed in the medium and longer wavelengths. Similarly, Miller proposed that, "the illumination color should be matched as closely as possible to the reflected color of the artefact," to prevent the color of an artwork from fading (Miller, 1993). However, matching "illumination color" with "reflected color" would shift the color appearance of the art (e.g., a red painting would appear very saturated in

* Corresponding author.
E-mail address: smayorga@ucm.es (S. Mayorga).

https://doi.org/10.1016/j.daach.2019.e00128
Received 18 June 2019; Received in revised form 5 November 2019; Accepted 22 November 2019

Abbreviations

AC	Printed picture
b	Constant determined in the Berlin model
CIE	International Commission on Illumination
CIEDE2000	Color-difference formula
DFK-72AUC02-F	CCD Camera
D_{PK}	Real spectral emission projector
$FI_{(x,y,rgb)}$	Algorithm three-dimensional matrix
GRF	Global Risk Factor
H_{dm}	Damage factor
JND	Just-noticeable difference
K	Adjustment parameter for R, G and B
$L^*a^*b^*$	Color space
LED	Light Emitting Diode
MF	Merit Function
P'_{PK}	Emitted spectrum from each pixel of the R, G and B channels of the LED projector
P_{cal}	Values corresponding to the amount of RGB of each frame
PK	Optoma® PK320 RGB LED projector
$S(\lambda)$	Relative spectral responsibility
SPD	Spectral power distribution
S_{PK}	The calculated spectral power distribution of the PK projector
$S_{reference}(\lambda)$	Spectral power distribution projector with R = G = B = 0.5
β_1	Optimized the color differences
β_2	Evaluated the damage caused by lighting
SURF	Speeded up robust feature algorithm
T	Parameters of the transformation
$w_{\beta 1}$	weight color difference
$w_{\beta 2}$	weight damage function
$Z(\lambda)$	Projector factor that relates the spectral measurements with those calculated
Z	Projector calibration matrix
ΔE_{00}	Minimum color difference with MF
$\delta_{relative}$	Relative light absorption
ρ_{AC}	Printed copies pictures reflectance

color under red light). Therefore, the proposal would work if the illumination color is not "matched with reflected color," but instead reverse-engineered to make objects appear the as they do under a reference illuminant, while minimizing light absorption.

A light projection system, that uses sensors to detect object colors (spectral reflectance functions) and emits spectrally optimized light to reduce the energy absorbed by the artwork, has been proposed (de Luna et al., 2015; Durmus and Davis, 2015). Investigations focused on architectural applications have shown that optimizing theoretical test SPDs to minimize the light absorbed by objects can reduce energy consumption from 38% to 44% without altering color appearance (Durmus and Davis, 2015). Double-peak theoretical spectra can further increase energy savings, up to 71% (Durmus and Davis, 2015). Computational simulations have shown that optimizing spectra to reduce light absorption decreases damage from 19% to 47% for single-color paintings (Durmus et al., 2018). Visual experiments showed that participants found single-colored real objects under optimized lighting and reference white light sources to appear equally natural and attractive (Durmus and Davis, 2017). Studies have also investigated the use of optimized lighting systems, including daylight and LED applications, in museums to save energy and, therefore, help reduce energy dependence and pollution (De-Graaf et al., 2013; Mueller, 2013; Mayorga et al., 2016; Al-Sallal et al., 2018).

Other researchers have used spectral optimization methods to reduce damage to artwork (Berns, 2011; Delgado et al., 2011) and restore the faded colors of museum artefacts (Viénot et al., 2011) by illuminating them with customized spectra. With some new techniques, art conservators can use light to restore the faded appearance of a masterpiece to its original state, as was done for Rothko's painting (Hecht, 2015). Projecting the original color of the painting, which was obtained thanks to the existence of slides of the original. This was done by projecting the original (non-faded) color of the painting, which was obtained from slides of the original. A projection system projects a compensation image on the original canvas to obtain a restored color appearance (Stenger et al., 2016). Berns used spectral calculations to create adjustment curves, where segmented portions of an object's image were translated in color (Berns, 2019). The absorption-minimization concept can be applied to museum lighting to reduce damage to sensitive materials, as well as to restore the appearance of already-damaged artwork.

Here, the construction of a point-by-point light projection system is described and its abilities to reduce damage from optical radiation and maintain the color quality of a multi-colored painting are quantified. The presented work is based, therefore, on the metameric colors, which are colors that appear the same to a human observer but have different SPDs (Schanda, 2007).

2. Methods

The system developed in this work consists in the characterization and processing of the spectral reflectance of the artwork in its current state and in its objective state to be achieved, so that the system can recover its color and control damage point by point. The following flow diagram (Fig. 1) the optimization process is described, from the characterization of the paint until obtaining better final illuminant for reconstruction and lighting of the same, causing the least possible damage.

A prototype of the point-by-point light projection system has been constructed using a calibrated red-green-blue (RGB) projector, multispectral filters and a computer system. A multispectral imaging camera was used to recover the spectral reflectance function of an oil painting reproduced in a printed copy derived from a photograph. An RGB projector was calibrated to emit light to each pixel of the printed picture, that depicts an aged version of the painting, using an optimization algorithm and a merit function (MF) to develop a light projection system that is capable of:

- *Obtain a good color quality of the printed picture*: The appearance of color between the printed copy illuminated with an International Commission on Illumination (CIE) daylight D65 reference and the printed copy color visually restored with the daylight projection system must be minimal. The reference illuminant D65 was used because it is represents daylight at 6500 K which represents the lighting conditions where the painter created the artwork (Phillips, 1912). The color difference (ΔE_{00}) was calculated in CIE 1976 $L^*a^*b^*$ using the CIEDE2000 formula (CIE, 2004), because the formula provides an improved estimation of industrial color differences (G. Sharma, 2005) where $\Delta E_{00} = 1$ is a just-noticeable difference (JND) under controlled laboratory conditions (Fechner, 1860; Fairchild, 2013).
- *Reduce damage of the artworks*: The Berlin model (CIE, 2004), which determines the damage caused to different materials (H_{dm}) from the spectral irradiance of illumination, was used to minimize the damage caused by optical radiation. Damage factor (H_{dm}) depends on the SPD and radiant flux of the illuminant, as well as the responsivity of the illuminated material.

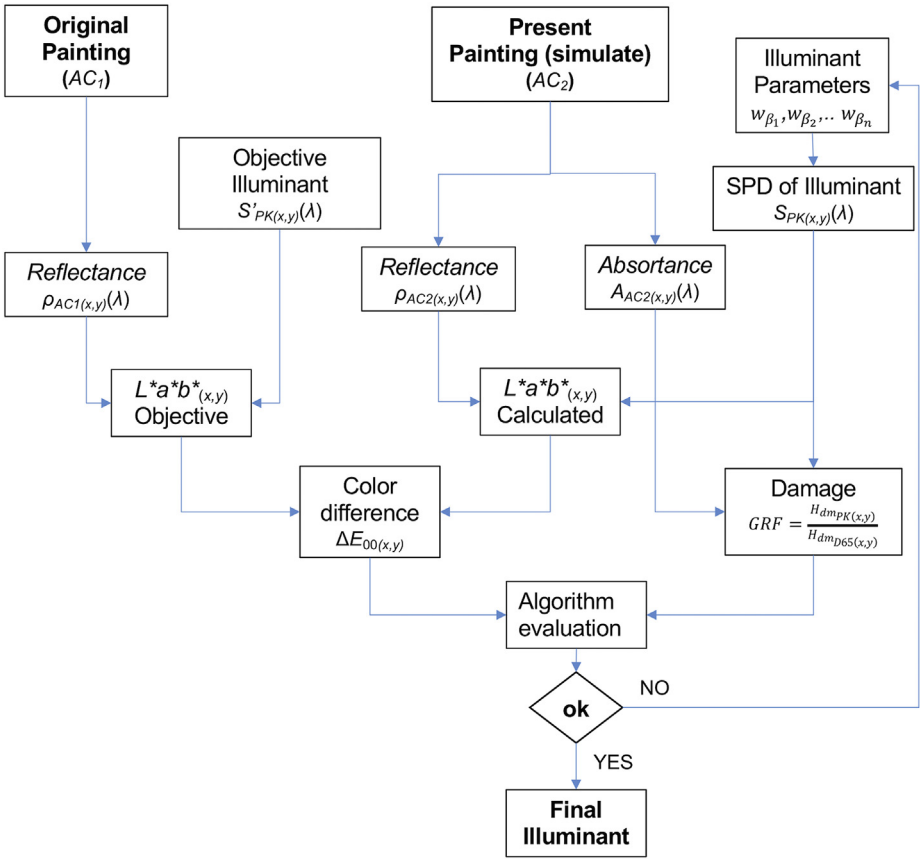

Fig. 1. Flow diagram, the steps of the optimization process for obtaining better final illuminant are described.

2.1. Color difference of the printed copies of picture

In this research, a digital archival image of Joaquín Sorolla's painting, "*Walk on the beach*", 1909 (provided by the Sorolla Museum Foundation inv. 834), was used to generate two printed copies, as shown in Fig. 2(a) and (b). They were printed with a Xerox 550 color printer with the same characteristics.

The digital archive was digitally changed with a filter using MATLAB® to simulate the photochemical aging process caused by light radiation, corresponding to AC_2 as shown in Fig. 2(b). The printed copy AC_1 is the digital archive given by the Sorolla Museum and served as a control to simulate an ideal color characteristic of the painting as shown in Fig. 2(a).

The aim of this investigation is to illuminate the printed copy AC_2 with the light projection system developed such that it has the color appearance of the undamaged AC_1. The goal is to demonstrate that, following a certain method and with the necessary information about the color and reflectance of the artwork, a light projection system can be developed that, when applied to real artwork, minimizes the damage and improves the color appearance. Fig. 2(c) shows the CIE 1976 $L^*a^*b^*$ coordinates calculated for each of the printed copies when illuminated by D65 illuminant.

The $L^*a^*b^*$ values were used to calculate the differences in color between the two images, to achieve the desired aging effect. The color difference created between the two printed pictures was such that the difference would be clearly noticeable to an observer ($1.0<\Delta E_{00}<20$). The color difference ΔE_{00} between the two printed copies was calculated with CIEDE2000, obtaining the values shown in Fig. 3. The average value was $\Delta E_{00} = 8.85$.

2.2. Spectral characterization of the printed pictures

In artwork conservation, the original work of art is generally used to determine differences in the spectral reflectance functions between the original object and reproductions, and to provide more accurate spectral reflectance estimation (Imai et al., 2000). When the original painting cannot be used as a reference, which is common in the case of old paintings, other techniques can be used to measure the reflectance function, such as restoring or cleaning selected small areas (Hwang et al., 2017) and characterizing the artwork by old photographic records (Stenger et al., 2016).

The spectral reflectance factors of the printed pictures (AC_1 and AC_2) were measured using high resolution monochromatic multispectral images (Shen et al., 2007; Murakami et al., 2012; Chane et al., 2013). Fig. 4(a) shows a diagram of the elements used for the acquisitions of multispectral images. Twenty multispectral images were taken with a QIMAGING® Retiga 1300 CCD high-resolution camera, which is sensitive in the visible spectral range, as shown in Fig. 4(b). Each monochromatic image captured a different spectral range, since twenty multispectral Thorlabs® band-pass filters were placed in front of the camera, each with a full width at half maximum of 10 nm ± 2 nm. The first image was captured with a 400 nm filter FB400-10, (i.e., the maximum transmittance of the second filter was at 420 nm FB420-10, and so on) up to 780 nm (FB780-10). In Fig. 3(b) the spectral behavior of the 400 nm filter with respect to visible radiation is shown as an example of the filters used. The lighting source was a standard 100 W Philips incandescent lamp, placed in front of the printed picture at a 45° angle relative the central axis of the system.

The spectral reflectance of each pixel, $\rho_{AC\,(x,y)}(\lambda)$ was acquired for AC_1 and AC_2 from 20 multispectral images. The size of each reflectance factor array of the multispectral image of the picture ($\rho_{AC1(x,y)}(\lambda)$, $\rho_{AC2(x,y)}(\lambda)$) was $x = 411$ pixels and $y = 450$ pixels. The image size (174.9 mm × 273.6 mm) corresponded to pixels with dimensions of 0.608 mm × 0.425 mm.

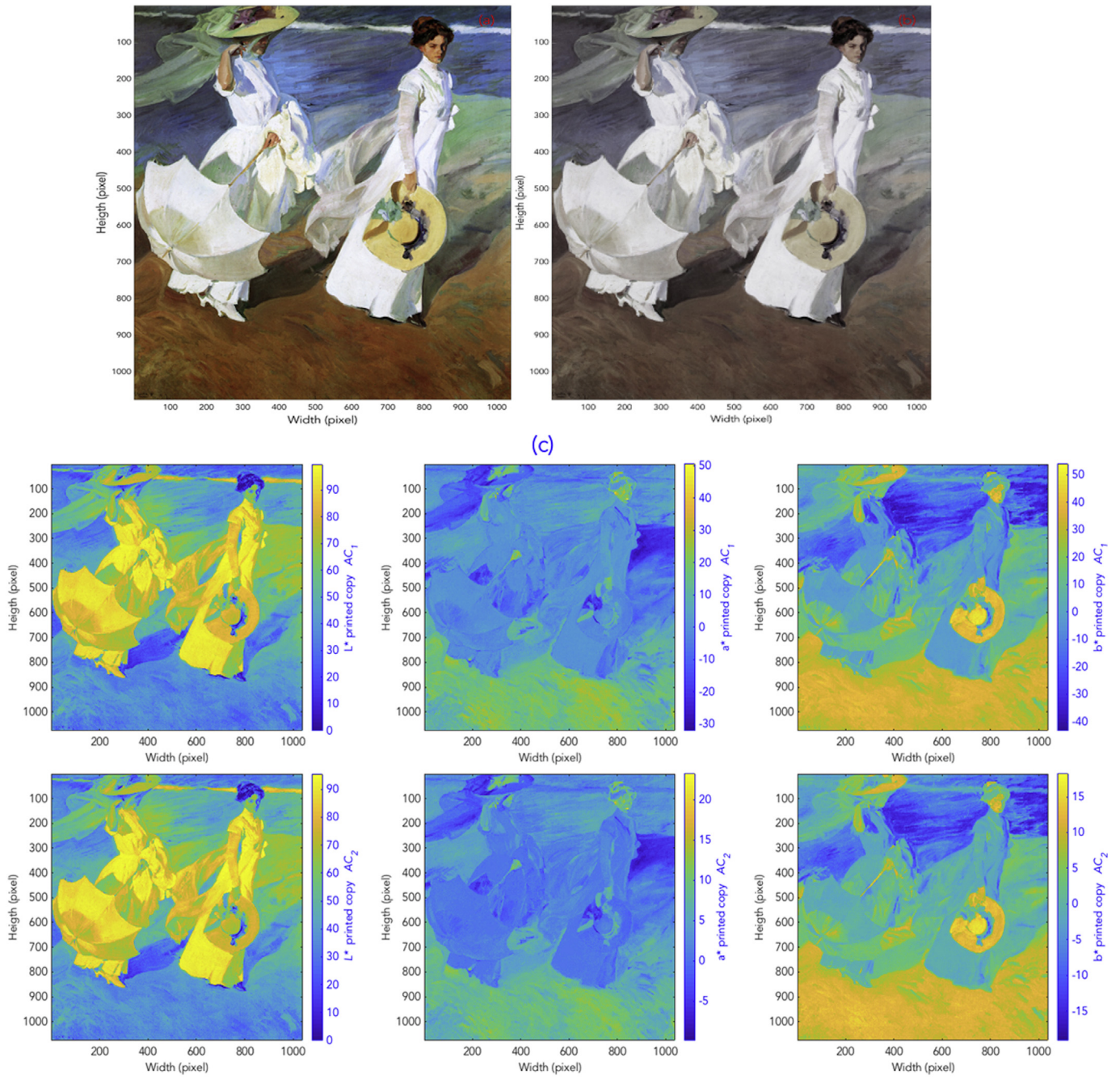

Fig. 2. "*Walk on the beach*" printed copies (a) The printed copy that simulates the reference painting was recovered from a digital archive courtesy of the Sorolla Museum Foundation inv. 834 (AC_1), (b) the digital archive (AC_1) was modified to appear faded using MATLAB® and was printed (AC_2). (c) Calculated color space coordinates ($L^*a^*b^*$) corresponding to the two images described in Fig. 2(a) and (b).

2.3. Projector calibration

An Optoma® *PK*320 RGB LED projector (*PK*) was used to illuminate the artificially aged printed picture (AC_2) to virtual restore its appearance (AC_1). The calculated spectral power distribution of the *PK* projector, $S_{PK(x,y)}(\lambda)$, for each pixel of the aged printed copy (AC_2) was

$$S_{PK_{(x,y)}}(\lambda) = K_{R(x,y)} \;\; R_{PK}(\lambda) + K_{G(x,y)} \;\; G_{PK}(\lambda) + K_{B(x,y)} \;\; B_{PK}(\lambda), \quad (1)$$

where $R_{PK}(\lambda)$, $G_{PK}(\lambda)$, $B_{PK}(\lambda)$ are the SPDs of the red, green and blue channels of the *PK*, as shown in Fig. 5, and $K_{R(x,y)}$, $K_{G(x,y)}$, $K_{B(x,y)}$ are intensity adjustment parameters ranging from 0.0 to 1.0.

Since the calculated SPD, $S_{PK(x,y)}(\lambda)$, was not identical to the real spectral emission of the *PK*, $D_{PK\,(x,y)}(\lambda)$, the projector was calibrated using a linear least-squared error approximation model to equate $S_{PK(x,y)}(\lambda)$ with $D_{PK(x,y)}(\lambda)$. Since a spectral, rather than colorimetric, calibration is required for this study, the calibration process differs from that usually employed for projectors and display screens (Simpson and Jansen, 1991; Marimont and Wandell, 1992; Quiroga et al., 1994). These models propose the following relationship between the output and input signal

$$D_{PK_{(x,y)}}(\lambda) = Z(\lambda) \;\; S_{PK_{(x,y)}}(\lambda), \quad (2)$$

where $Z(\lambda)$ is a dimensionless factor that relates the spectral measurements with those calculated. *PK* was been calibrated to calculate *Z*. Fig. 6(a) shows the diagram of the elements used for the calibration of the

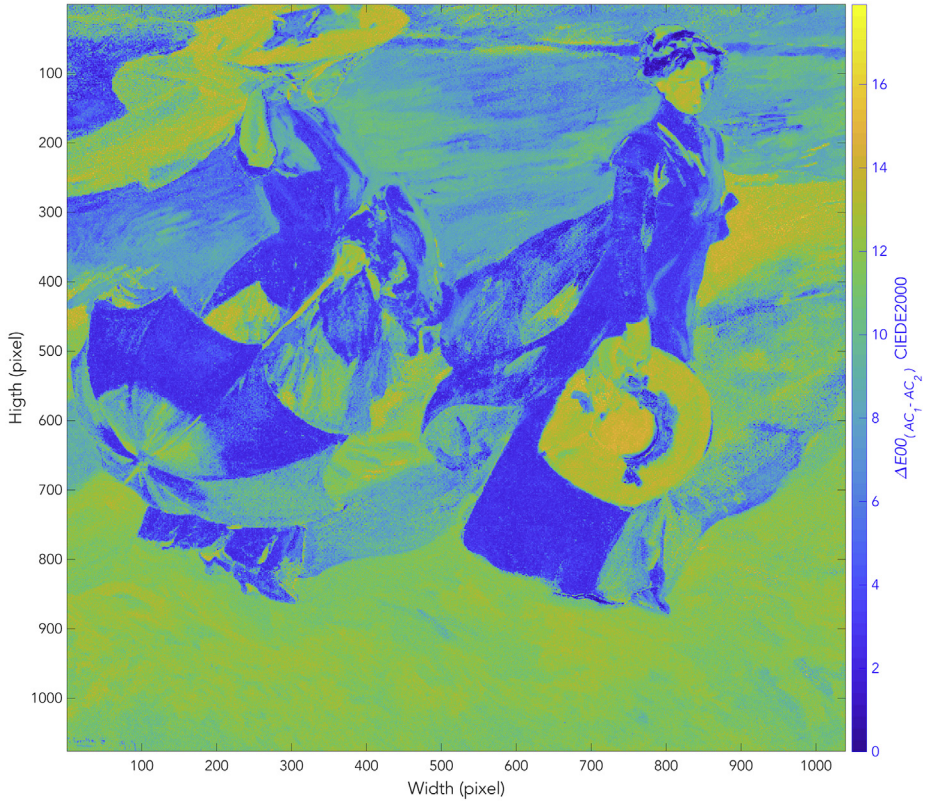

Fig. 3. CIEDE2000 ΔE_{00}. Image shows color differences between the two printed pictures, AC_1 and AC_2, before applying the developed light projection system.

PK.

An array of 512 pixels, shown in Fig. 6(b), was composed of a combination of different RGB values to covers the widest possible color gamut. An array, with a size of 512 × 3 pixels, P_{cal}, was formed

$$P_{cal} = \begin{bmatrix} P_{cal_R,(1)} & \cdots & P_{cal_R,(512)} \\ P_{cal_G,(1)} & \cdots & P_{cal_G,(512)} \\ P_{cal_B,(1)} & \cdots & P_{cal_B,(512)} \end{bmatrix}, \tag{3}$$

where $P_{cal\_R1\ \ldots\ 512}$ were the values corresponding to the amount of red (R) of each frame, $P_{cal\_G1\ \ldots}$ were the green (G) values and $P_{cal\_B1\cdots B512}$, were the blue (B) values.

The array P_{cal} was projected on to a white screen with *PK*. Using the Photo Research SpectraScan® Spectroradiometer PR655, 512 non-contact measurements were made at each point of each projected frame. These values were corrected, by taking the spectral reflectance function of the screen ($\rho_{screen\_diffuser} = 0.95$) into account, and the resulting values were the spectral emission of the projector for each frame, $D_{PK}(\lambda)$, which, for the calibration calculations, was divided into the three emission channels of the projector, R, G and B, independently.

$$P'_{PK_{R(1,..512)}}(\lambda) = D_{PK_{R(1,..512)}}(\lambda)\ R_{PK}(\lambda), \tag{4}$$

$$P'_{PK_{G(1,..512)}}(\lambda) = D_{PK_{G(1,..512)}}(\lambda)\ \ G_{PK}(\lambda), \tag{5}$$

$$P'_{PK_{B(1,..512)}}(\lambda) = D_{PK_{B(1,..512)}}(\lambda)\ \ B_{PK}(\lambda), \tag{6}$$

where $P'_{PK\_R(1,512)}(\lambda)$, $P'_{PK\_G(1,512)}(\lambda)$ and $P'_{PK\_B(1,512)}(\lambda)$ represent the spectrum emitted by from each pixel of the red, green and blue channels of the LED projector, respectively. $D_{PK}(\lambda)$ is the sum of the spectral values measured for each channel and for each frame

$$D_{PK(1,...512)}(\lambda) = P_{PK_{R(1,...512)}}(\lambda) + P_{PK_{G(1,...512)}}(\lambda) + P_{PK_{B(1,...512)}}(\lambda). \tag{7}$$

The measured values (spectral data of each frame) and the calculated values (*R*, *G* and *B* data of each frame) were unified in the same dimensional space to characterize the relationship between them (*Z*). The spectral values from equations (4)–(6) were transformed to *R*, *G* and *B* tristimulus values ($P'_{PK\_R(n)}$, $P'_{PK\_G(n)}$, $P'_{PK\_B(n)}$) using the CIE 1931 standard observer (CIE, 2004; Schanda, 2007). As a result, D_{PK} can be expressed as a 512 × 3 element array of RGB values

$$D_{PK} = \begin{bmatrix} P'_{PK_R,(1)} & \cdots & P_{cal_R,(512)} \\ P'_{cal_G,(1)} & \cdots & P_{cal_G,(512)} \\ P'_{cal_B,(1)} & \cdots & P_{cal_B,(512)} \end{bmatrix}, \tag{8}$$

where, $P'_{PK\_R(1)\ \ldots\ (512)}$, $P'_{PK\_G(1)\ \ldots\ (512)}$ and $P'_{PK\_B(1)\ \ldots\ (512)}$ are the *R*, *G* and *B* values of each pixel (1–512).

D_{PK} and P_{cal} were used to calculate the projection system's deviation from the input signal employing the least squares adjustment of the linear transformation (Quiroga et al., 1994)

$$D_{PK} = ZP_{cal}, \tag{9}$$

where *Z* is a 3 × 3 matrix that solves the RGB deviation of the *PK* for each pixel of the output signal.

Matrix *Z* was obtained by the least squares' adjustment

$$\widehat{Z} = \left(P_{cal}P_{cal}^T\right)^{-1}P_{cal}^T D_{PK}, \tag{10}$$

and the values obtained from the calibration of the projection system were

$$\widehat{Z} = \begin{bmatrix} 0.8955 & -0.1972 & 0.0688 \\ -0.1306 & 0.9272 & -0.1078 \\ 0.0615 & -0.0342 & 0.9039 \end{bmatrix}, \tag{11}$$

In order to check the validity of the adjustment, the mean squared error (MSE) of the calibration model for each channel ($\mathcal{E}_R = 0.0371$, $\mathcal{E}_G =$

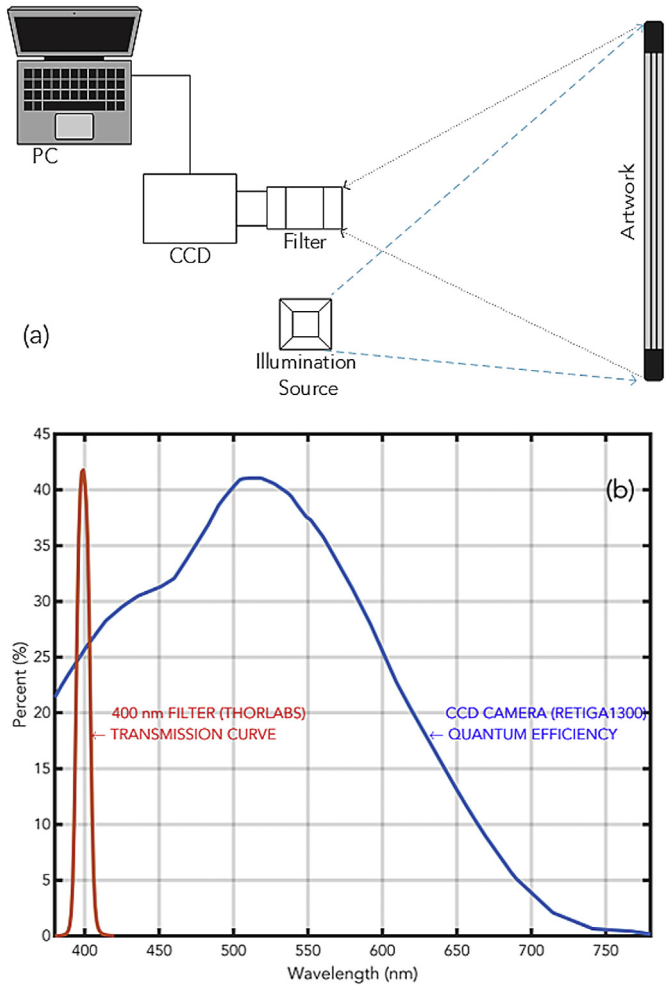

Fig. 4. Spectral characterization (a) Multispectral images of the printed pictures were taken with a QIMAGING® Retiga 1300 CCD camera and 20 Thorlabs® filters, with peak spectral transmittances from 400 nm to 780 nm. Printed pictures were illuminated with a lamp with spectral emission similar to CIE illuminant A (incandescent lamp), and computer software was used to record measurements and process data. (b) The spectral sensitivity of the QIMAGING® Retiga 1300 CCD camera and transmission characteristics of the Thorlabs® filter. The spectral transmission function shown in the graph corresponds to one of the filters used, with peak transmittance at 400 nm.

0.0358, and $\mathcal{E}_B = 0.0665$), and their standard deviations ($\sigma_R = 0.0021$, $\sigma_G = 0.0043$, and $\sigma_B = 0.0021$) were calculated.

2.4. Merit function

A merit function (MF) is a weighted combination of minimization objectives (i.e., parameters to be minimized) in multi-objective optimizations. Here, a dynamic MF (Fernandez-Balbuena et al., 2015) was applied to optimize the lighting parameters (color appearance of artificially aged printed picture and damage factor). Considering the major influence that the illuminant has on the appreciation of color in the exhibition of art, it was necessary to minimize the difference in color appearance between the reference and the test lighting conditions. The MF (β_1) optimized the color differences, CIEDE2000 $\Delta E_{00(x,y)}$ (CIE, 2004)

$$\beta_1 = \Delta E_{00_{(x,y)}} = \sqrt{\left(\frac{\Delta L'}{K_L S_L}\right)^2 + \left(\frac{\Delta C'}{K_C S_C}\right)^2 + \left(\frac{\Delta H'}{K_H S_H}\right)^2 + R_T\left(\frac{\Delta C'}{K_C S_C}\right)\left(\frac{\Delta H'}{K_H S_H}\right)}, \tag{12}$$

where $\Delta L'$, $\Delta C'$ and $\Delta H'$ are the differences the lightness (L'), chroma (C') and hue (H') between the coordinates of a pixel in the printed pictures under the reference condition (D65 illuminant) and test condition (optimized lighting). The values obtained from the reflectance of printed pictures, $\rho_{AC}(\lambda)$, were transformed using CIEDE2000, and the MF created iterations until a minimum ΔE_{00} was obtained.

In addition to color difference, another MF (β_2) evaluated the damage caused by lighting. In this model a numerical measured standard value is used, the Global Risk Factor (GRF) (Mayorga et al., 2016), which compares the D65 illuminant and the *PK* illumination system in a way that is easy to interpret. The value obtained for the GRF indicates the number of times that the damage to the illuminated area equals or exceeds the damage caused by the D65 illuminant, with a value of unity for areas having the same damage factor (H_{dm}).

$$\beta_2 = GRF = \frac{H_{dm_{PK(x,y)}}}{H_{dm_{D65(x,y)}}}, \tag{13}$$

where GRF is dimensionless, and H_{dm_PK} is the effective radiant exposure of the projector and H_{dm_D65} is the effective radiant exposure of the D65 illuminant, in Whm^{-2}.

$$H_{dm_{PK(x,y)}} = \iint_{\lambda,t} E_{PK}(\lambda)(t)\, S(\lambda)\, A_{\mathrm{PK}_{x,y}}(\lambda)\, d(\lambda)\, d(t), \tag{14}$$

$$H_{dm_{D65(x,y)}} = \iint_{\lambda,t} E_{D65}(\lambda)(t)\, S(\lambda)\, A_{\mathrm{D65}_{x,y}}(\lambda)\, d(\lambda)\, d(t), \tag{15}$$

where $E(\lambda)$ is the spectral irradiance of the incident light, in Wm^{-2}, on each pixel (x, y) for D65 or *PK*, $A(\lambda)$ is the absorbance function for each illuminant for each pixel (x, y) of the printed picture and $S(\lambda)$ is the relative spectral responsivity of the painting normalized a 300 nm, represented by an exponential function of the form

$$S(\lambda) = exp[-b(\lambda - 300)], \tag{16}$$

where $b = 0.0115$ for oil paints on canvas (CIE, 2004). Although the picture used here is printed on paper, the oil paint sensitivity data are used, since the aim of the research is to eventually used this method to reduce damage to real works of art.

When the two objective functions are combined, the final MF is expressed as

$$MF = (w_{\beta_1}\beta_1 + w_{\beta_2}\beta_2), \tag{17}$$

where $w_{\beta 1}$ and $w_{\beta 2}$ are weights ranging from 0.0 to 1.0. β_1 and β_2 are optimized separately, to minimize their values as much as possible. The optimization is conditioned by the weights ($w_{\beta 1}$ and $w_{\beta 2}$) assigned to each β. The MF results determines when the calculation stops. The freedom of being able to modify the weights to give more importance to one of the factors (damage or color difference) provides flexibility to this methodology.

2.5. Optimization algorithm

A Nelder-Mead simplex algorithm (Nelder and Mead, 1965) was used to optimize the color appearance and minimize damage caused by optical radiation. This optimization method, based on the simplex concept (Lagarias et al., 1998), is a technique commonly used to minimize a multi-objective function, and it has been shown to be a suitable method for the optimization of lighting systems (Lin et al., 2013).

The algorithm calculated the optimal spectral power distribution and the intensity of each point in the image $S_{AC(x,y)}(\lambda)$. These values result from adjusting the K parameters (K_R, K_G, and K_B) described in Eq. (1). The calculation started with $S_{reference}(\lambda)$, which was defined as $K_R = 0.5$, $K_G = 0.5$ and $K_B = 0.5$. K values were changed in different sequences, which did not influence the result. The optimization terminated when

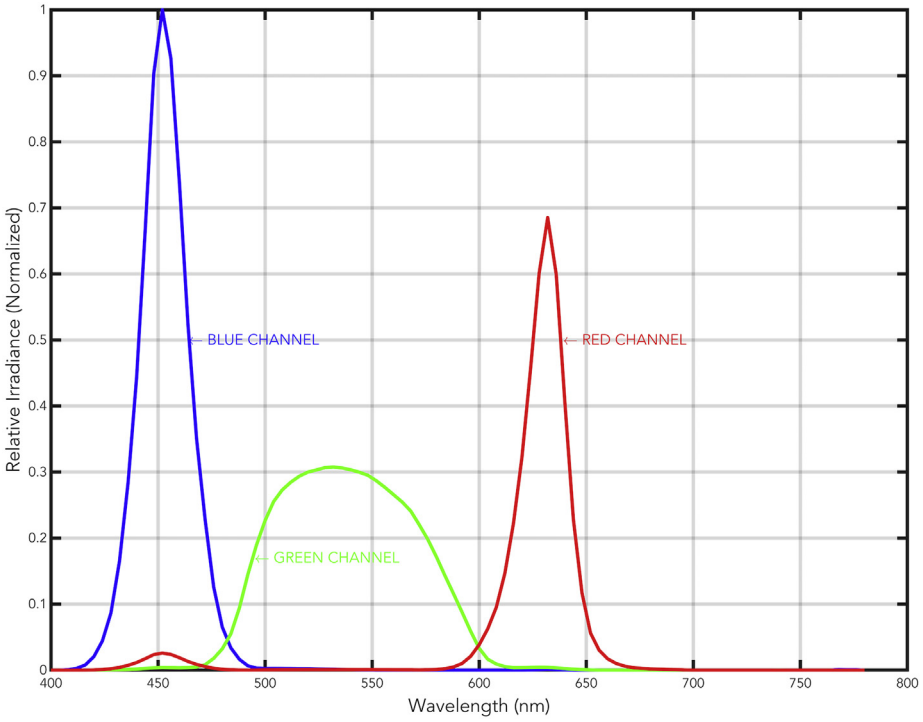

Fig. 5. Spectral curves of the Optoma® *PK320* projector. The spectral power distribution of the RGB channels of the *PK* projector at their maximum intensities: $R_{PK}(\lambda)$ when $K_R = 1.0$ for the red channel, $G_{PK}(\lambda)$ when $K_G = 1.0$ for the green channel, and $B_{PK}(\lambda)$ when $K_B = 1.0$ for the blue channel. To obtain the SPD of the projector, a fixed image of each color was projected onto a diffuse white screen with a measured reflectance of 95%. The measurements were obtained with a Photo Research SpectraScan® Spectroradiometer PR655. (For interpretation of the references to color in this figure legend, the reader is referred to the Web version of this article.)

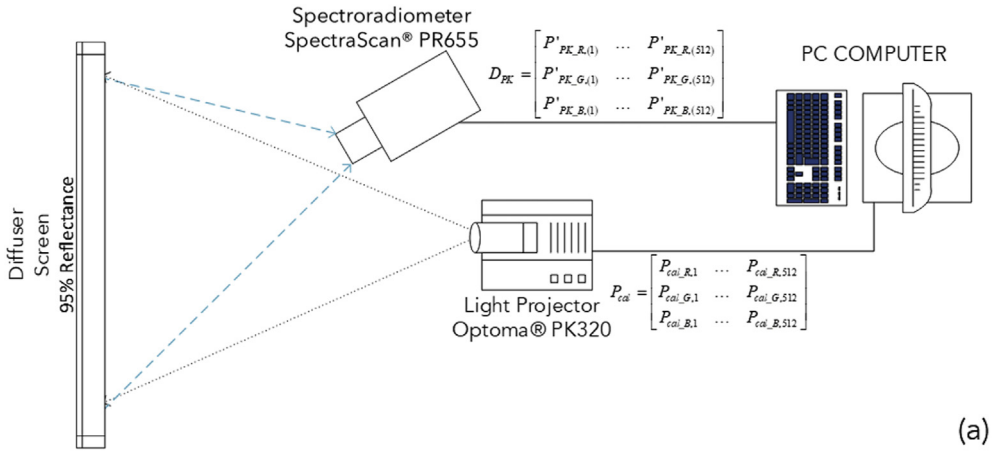

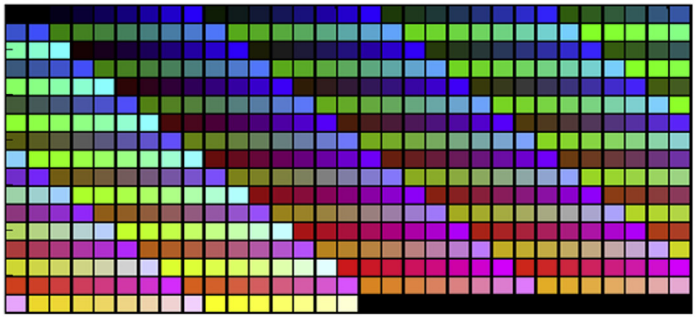

Fig. 6. Diagram of the calibration equipment and process. (a) A diffuse white screen with 95% reflectance, a Photo Research SpectraScan® Spectroradiometer PR655 and a computer were used to calibrate the RGB Optoma® PK320 projector, and (b) an array of 512 pixels.

optimal values for each pixel were reached, the predefined maximum iterations were reached, the constraint functions could not be reduced any further, or the end of the sequence was reached.

2.6. Optimization of lighting

The calculated light emission of the projector is an optimized value, with the merit function of the K parameters (K_R, K_G, and K_B) for the

selected pixel that, when the spectral profile of the *PK* projector is applied, produces a light emission that causes minimal damage and minimal color difference between the aged and non-aged printed pictures. The final values of the *K* parameters (K_R, K_G, and K_B) are the R, G and B of each pixel.

2.7. Lighting projection

The optimized lighting calculated by the algorithm is a three-dimensional matrix, $FI_{(x,y,rgb)}$, where the third dimension represents the intensities of the *R, G* and *B* channels of the projector. The spatial coordinates (*x, y*) correspond to the reference system defined by the position and spectral reflectance obtained by multispectral imaging.

Since the projector had to be positioned slightly off-axis to the printed copy picture, the projected image was expected to be distorted due to the change of perspective (i.e., keystone effect), as well as the difference in the optical characteristics of the acquisition and projection systems (i.e., focus, magnification and optical distortions).

In theory, it is possible to accurately determine the position, orientation and optical characteristics of the artwork, acquisition system and projector, as shown in Fig. 7. These aspects (position, orientation and optical characteristics) are necessary to pre-calculate the inverse transformation function that compensates for all deformations and distortions. However, this would impose extremely strict experimental requirements in terms of the accuracy of the measurements and the stability of the system.

To avoid these strict requirements, a calibration method was developed based on triangulation techniques to infer the geometric parameters of all the elements by projecting circular beams of light. The system was inspired by structured light projection techniques where the correspondences between the projected light patterns and their images are characterized, also known as the correspondence problem in computer vision (Capel and Zisserman, 2003). An added difficulty was that, in the projection plane there was an object with a variable reflectance distribution, which complicated the detection and automatic indexing of the projected structures and prevented the use of the traditional chessboard pattern. Therefore, a temporal modulation pattern was projected for identification and labeling. This process requires additional processing time but increases the accuracy of the calibration using sub-pixel precision techniques (Bouguet, 2012).

Using the MATLAB® image processing toolbox, the coordinates of the centroids of the projected patterns in the projection plane (x_p, y_p) and the parameters of the transformation *T* were obtained. The data were used to establish the correspondence with the array of the projected theoretical positions (*x,y*). The transformation *T* was obtained by a two-stage process. First, an approximate initial estimate was generated, in which a projective transformation was assumed (straight lines remain straight, and parallel lines converge towards a vanishing point). Subsequently, *T* was refined with a polynomial adjustment, which accounted for possible distortions introduced by the optical systems (Zhang, 2000). The inverse transformation, T^{-1}, was applied to the optimized lighting condition, $S'_{AC(x,y)}(\lambda)$, so that the projected image was $T^{-1}[S_{AC(x,y)}(\lambda)]$, and the resulting signal became $S'_{AC(x,y)}(\lambda)$.

The estimation of the transformation, *T*, was used to correct the distortions in the three-dimensional composition formed by the projector, the camera and the printed picture. However, the origin coordinates acquired by the spectroradiometer must be precisely matched with the specific position of the printed pictures in the projection plane.

Manual adjustments were omitted for greater precision in the process, and artificial vision techniques, based on the search for correspondence between pairs of images (Vincent and Laganière, 2005), were used to detect the exact position of the printed pictures. An additional advantage of this process is the automatic readjustment of the system, which allows maintenance of the printed picture and the exhibition space. An algorithm called the speeded up robust features (SURF) detector (Bay et al., 2008) was used to detect and describe the points of interest of an image, which has a good sensitivity to position and scale changes.

Once the most relevant points of interest were detected, they were paired based on the similarity of the detected characteristics, while pairs that did not exceed predetermined threshold limits were discarded.

The control of the position of the printed pictures and the projector was carried out by a DFK-72AUC02-F Imaging Source CCD camera, as shown in Fig. 8. The camera has an autofocus function and spatial resolution of 2592 × 1944 pixels. It transferred the information to a mini PC, which ran the artificial vision algorithm. With this artificial vision algorithm, it was possible to obtain accurate positioning of the image within 0.5 pixels. Software was developed for the proposed practical example, which analyzed and performed corrections.

3. Results

The light projection system optimized the lighting from the RGB projector to minimize the color difference between the reference photography and restored printed copy picture. The light absorption and the color quality of the printed copy picture under D65 illuminant and optimized lighting were quantified.

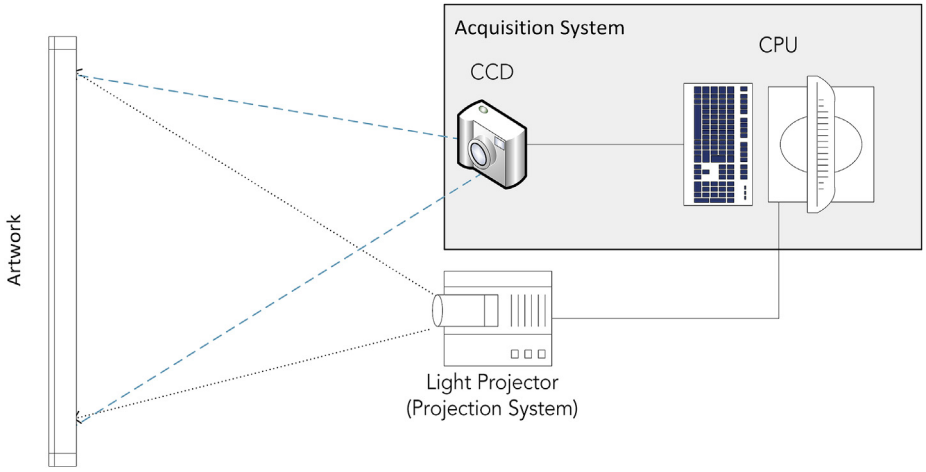

Fig. 7. Diagram of the light projection system, consisting of a printed picture, an image acquisition system (a CCD camera and a PC), and a projector. Images were taken with the CCD camera and were spatially tested using the software developed by the researchers. The signal was adjusted in real time, so that the light was always focused on the surface of the illuminated printed picture.

Fig. 8. Proposed light projection system, consisting of the Optoma® PK320 projector, that emits light onto of the painting, a DFK-72AUC02-F CCD camera, which was used to correct the spatial position of the system with respect to the illuminated printed picture, and the PC that processes the CCD data and applies the artificial vision algorithm to correct the image emitted by the projector according to the location of the printed picture.

3.1. Optimized lighting emitted by the projector to the printed picture AC_2

The values obtained for the R, G and B of each pixel are represented in Fig. 9(a). The damage and color resulting from the light emitted by the light projection system depends on the R, G and B values obtained with the merit function, the spectral profile of the projector, the calibration of the projector and the lighting projection. Through these processes, non-invasive virtual photonic restoration was carried out to improve the appearance of the artificially aged printed image, as shown in Fig. 9(b), achieving a visual recovery of the color without physical intervention, as shown in Fig. 9(c).

3.2. Minimization of color difference and damage obtained with the merit function

The results obtained with the merit function improved the performance of light projection system by approaching the ideal composition of reflected light to restore the appearance of the artificially aged printed picture. The resulting color differences for each pixel between the original printed picture AC_2 and the artificially damaged printed picture AC_2 when illuminated by optimized test lighting ($\Delta E_{00(x,y)}$) are shown in Fig. 10(a). The average color difference suggests that the printed picture AC_2 would appear indistinguishable under the optimized lighting condition from printed picture AC_1 when illumination by the reference lighting condition. However, in 458 pixels (less than 0.25% of the image), the color difference was greater than 1.0.

Fig. 3 compares the appearance of between the two printed pictures (AC_1 and AC_2) when both are illuminated by D65, with an average color difference between the images of $\Delta E_{00} = 8.85$. With the MF optimization, the color difference between AC_1 and "AC_2 restored," as shown in Fig. 9(c), is $\Delta E_{00(x,y)} = 0.27$. As shown in Fig. 10(a), the average color difference has been reduced 33 times.

Fig. 10(b) and (c) show the calculated damage factor H_{dm} value of the *PK* for each pixel and the H_{dm} value of the D65 illuminant for each pixel respectively. The results show that the damage factor with the illuminant D65 is much greater than with the optimized light projection system developed in the investigation.

The optimization algorithm used two objective functions (color difference, ΔE_{00}, and damage factor, H_{dm}). The optimization algorithm used two objective functions (color difference, ΔE_{00}, and damage factor, H_{dm}). The optimization algorithm minimized the effective irradiance, H_{dm}, and color differences within 40 iterations. The MF implemented is a very flexible tool, as only a small change in the value of the weights is needed to modify the characteristics of the light projection system. An increase in weight directly increases the importance of the selected variable. In the optimization process used here, the quality of the color appearance was given a greater weight than damage ($w_{\beta 1} = 0.8$ and $w_{\beta 2} = 0.2$) to decrease color differences.

Fig. 11 shows the results of the average merit function for all the pixels, based on the optimization iterations for damage and color difference caused by the illumination, optimized for *PK*. It has been verified that increasing the number of iterations does not improve the performance of the developed light projection system. The recommended number of iterations was $n = 40$, since there were no improvements with additional iterations. This has been tested by increasing the number of iterations (e.g., 60, 70) and no appreciable decrease in the color difference or damage was been detected.

3.3. Damage by optical radiation

Since the Berlin Model recommended by CIE 157 (CIE, 2004) does not fully capture the relationship between spectral reflectance and damage, relative light absorption calculations were performed to quantify the damage caused by light absorption. To develop a complete understanding of damage produced by light, the both the Berlin Model and a relative light absorption ($\delta_{relative}$) have been considered in the results.

The light absorbed by each pigment under optimized lighting was compared to the amount of light absorbed when illuminated by reference daylight and incandescent illuminants. A reference standard D65 illuminant was used in the color difference calculations to account for the lighting condition under which the artist created the painting (daylight). Incandescent was also used to calculate light absorption, since 51% of museums still use incandescent as the primary light source (Perrin et al., 2014).

The damage factor (H_{dm}) of the Berlin Model was used to calculate the relative damage to an oil painting represented by the printed picture. The average was $H_{dm\_PK} = 0.0185$ Whm^{-2} and the maximum was $H_{dm\_PK} = 0.0312$ Whm^{-2} when the picture was illuminated by the light projection system, as shown in Fig. 10(b). The average value was $H_{dm\_D65} = 0.2953$ Whm^{-2}, with a maximum of $H_{dm\_D65} = 0.4351$ Whm^{-2} when illuminated by D65, as shown in Fig. 10(c). When lit by illuminant A, the average value was $H_{dm\_illuA} = 0.3891$ Whm^{-2} and the maximum was $H_{dm\_illuA} = 0.5907$ Whm^{-2}.

Fig. 12 shows the GRF of the effective radiation from the projector compared to the two illuminants. The light projection system developed optimizes the projected SPD by taking into account absorbed energy and damage factor (H_{dm}). In this example, it has an average value that is 0.063 times the value for D65 illumination, as shown in Figs. 12(a), and 0.0483 times the value for illuminant A, as shown in Fig. 12(b).

When it is not possible to measure the spectral responsivity function of the materials, the damage evaluation must be applied without the reflectance information, $S(\lambda)$. In order to do this, relative light absorption ($\delta_{relative}$) is calculated

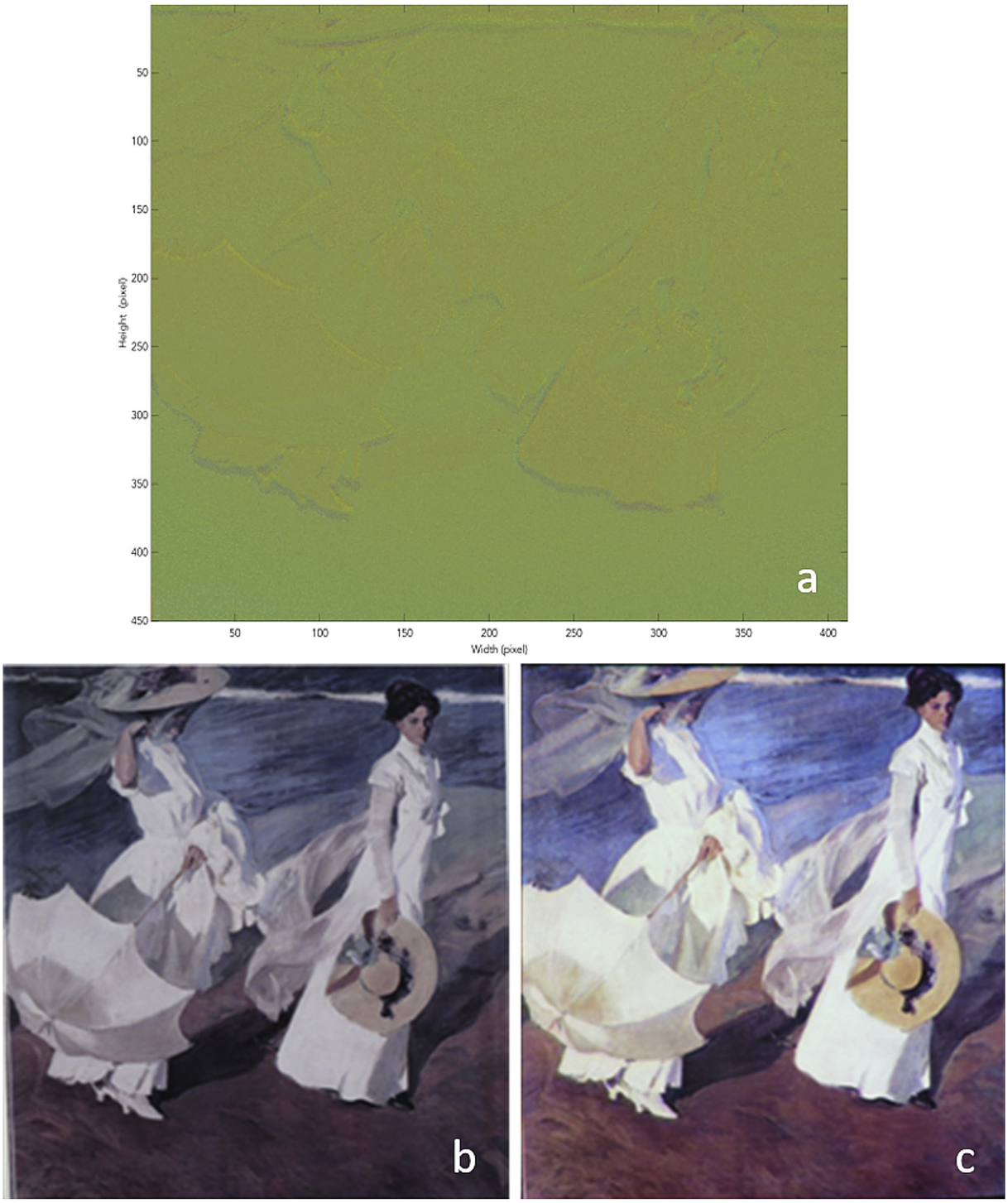

Fig. 9. Virtual photonic restoration (a) Shows the RGB value obtained with the merit function. With these RGB values, the artificially aged printed material has a minimum color difference and the damage is optimized (non-invasive virtual photonic restoration method). (b) The spatially and spectrally optimized lighting can enhance the color appearance of a faded printed picture shows AC_2 with artificial aging (c) shows the color appearance of AC_2 with the application of the non-invasive virtual photonic restoration method.

$$\delta_{relative} = \frac{\int S_{test(x,y)}(\lambda)(1-\rho(\lambda)_{(X,Y)})d\lambda}{\int S_{ref}(\lambda)(1-\rho(\lambda)_{(X,Y)})d\lambda}, \tag{18}$$

where $S_{test(x,y)}(\lambda)$ is the optimized SPD for each pixel, $S_{ref}(\lambda)$ is the SPD of the reference daylight illuminant, and $\rho(\lambda)_{(x,y)}$ is the spectral reflectance factor of each pixel. The amount of light reflected (weighted by the spectral luminous efficiency function) from the test and reference conditions were kept equal to prevent color appearance phenomena, such as the Hunt effect (colorfulness increase with luminance) (Hunt, 1952) and the Bezold-Brucke hue shift (hue shift with luminance) (Pridmore, 1999), and to ensure that reductions in light absorption were not the consequence of reduced painting brightness.

The amount of light absorbed by the printed copy picture ranged from 61% to 109%, compared to the reference daylight illuminant, as shown in Fig. 13(a). The average $\delta_{relative}$ was 82%, with a standard deviation of 6%. The amount of light absorption under the optimized SPD increased

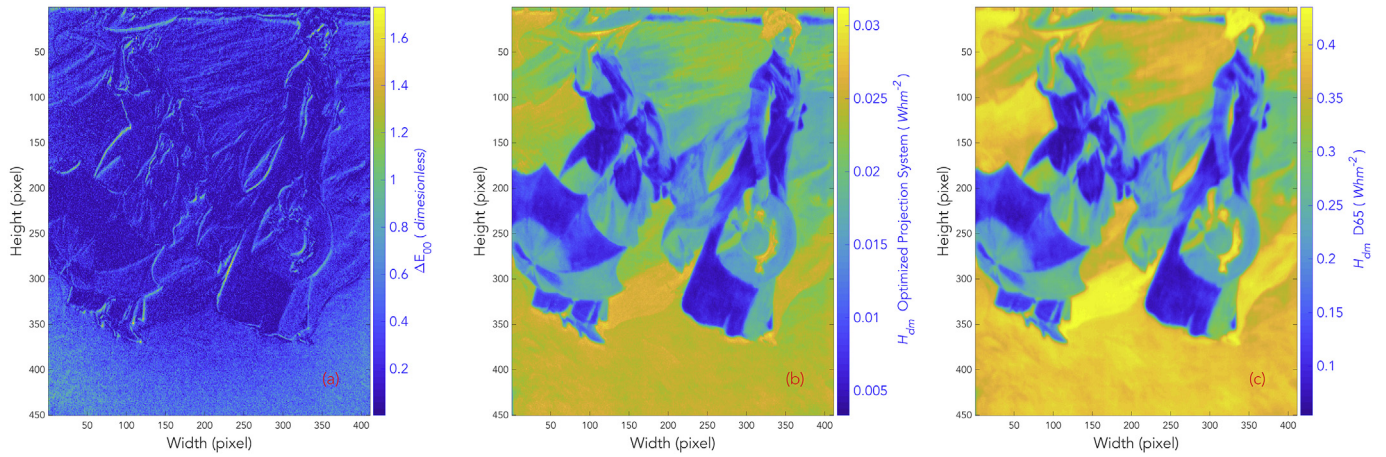

Fig. 10. MF results. (a) Shows the color difference, ΔE_{00}, for each pixel of the printed picture AC_2 illuminated by light projection system and AC_1 illuminated by reference illuminant D65. (b) Optimized H_{dm_PK} for each pixel with the light projection system developed (in Whm^{-2}). (c) Calculated H_{dm_d65} for each pixel for D65 illumination (Whm^{-2}), where H_{dm} (damage factor) is the effective irradiance that causes damage, which takes into account the spectrum of incident radiation and the relative spectral response of the receiving material for 1 h.

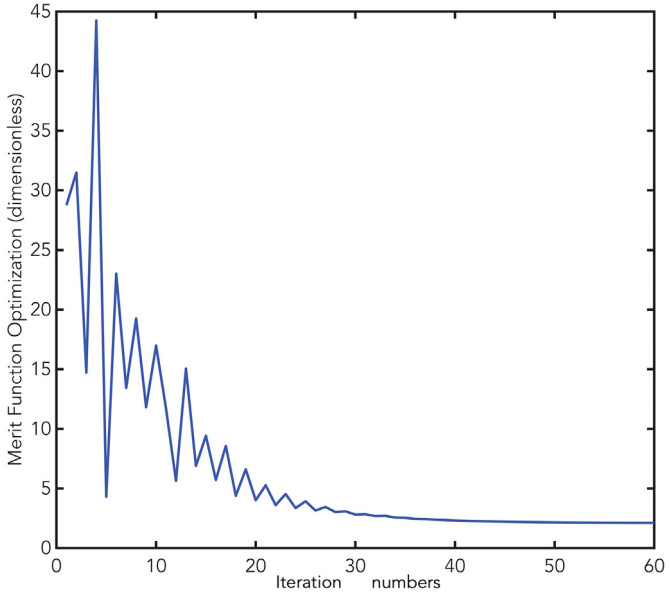

Fig. 11. MF iterations. The average damage and color difference for all the pixels of the printed picture, as a function of iteration number. The merit function continues to improve the performance of the light projection system up to iteration 35, on average. Therefore, 40 iterations were performed for each pixel.

for only 2113 pixels (out of 450 × 411 pixels), comprising approximately 1% of the image.

When the reference illuminant was incandescent, light absorption ranged from 33% to 127%. The average $\delta_{relative}$ was 63%, with a standard deviation of 12% (Fig. 13(b)). The amount of light absorption under the optimized SPD increased for only 4683 pixels (out of 450 × 411 pixels), which is around 2.5% of the image.

4. Discussion

This paper presents a methodology to enable non-invasive photonic restoration to obtain the best lighting for minimizing damage and maximizing color reproduction of a work of art, using a point by point spectral projection system. This methodology is tested on a printed picture, but it can also be implemented on different types of photoresponsivity medium (e.g., oil paintings, drawings, textiles, etc.).

The color degradation was simulated by a computer application to enable comparison to previous studies (Mayorga et al., 2016) and propose a complete methodology for developing a light projection system that visually restores the color of works of art with light. This example demonstrates that the proposed light projection system can alter the color of the printed picture AC_2, resulting in a virtual photonic restoration, yielding an excellent reproduction of non-aged printed picture AC_1.

This proposal is largely intended for application to certain specific cases in which most classic restoration techniques cannot be used. It has been demonstrated that the developed light projection system works correctly in the laboratory, with appreciable results, both in the improvement of the color appearance and in the reduction of the damage caused by the radiation. Nevertheless, this work must be improved for in situ applications, where it would be necessary to consider the art medium, its location, and to use more complex light sources than an RGB system. Additionally, more research is needed to develop a more comprehensive damage factor metric.

However, the proposed light projection system is functional and applicable, and its investment can be assumed if compared with the benefits that entail. The goal is to reach the works of art affected by a loss of color, where restorers and conservators do not recommend the use of invasive techniques because the advantages do not outweigh the damage caused. Another benefit that is achieved with this system is to delay further deterioration produced by lighting sources. The group has obtained a grant to implement this for a real picture from Dali entitled “Dos Figuras” and demonstrate it in Museo Reina Sofía in Madrid.

Although the calculations made involved in the process take time – in this example, given the size and resolution of the printed picture, it took approximately 4 h – this aspect wouldn’t meaningfully increase costs, since the calculations are only performed operation once and are automated.

The methodology used is transferable, with the necessary adaptations, to the personnel responsible for conservation in museums and art exhibitions, so that they can develop light projection systems adapted to the needs of particular works of art.

5. Conclusions

Degraded artwork can be photonic virtually restored using the proposed algorithms and hardware set-up. The damage caused to a work of art by optical radiation can be reduced by spectrally optimizing the light source emission.

Colorimetric calculations show that shifts in the color appearance of

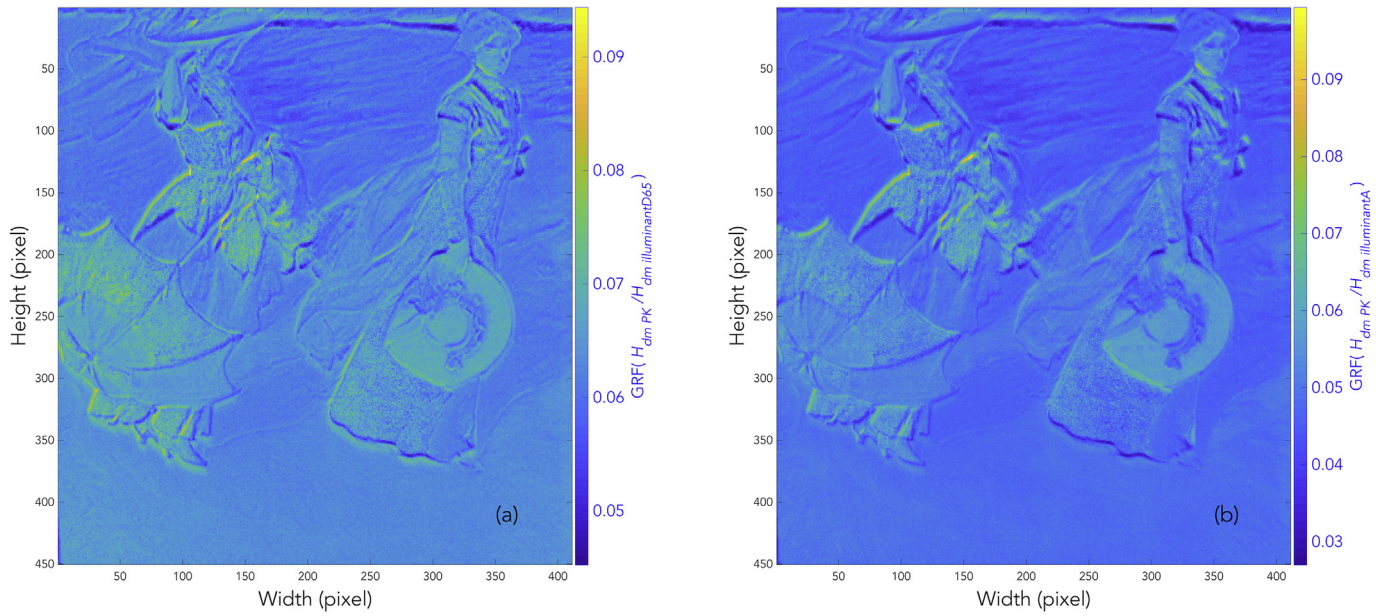

Fig. 12. GRF for optimized lighting compared to reference illuminants. Shows the GRF when the printed picture is illuminated with the projector compared to the D65 illuminant, both with the same illuminance (100 cd/m^{-2}). (b) Shows the GRF for the same picture illuminated with the projector compared to illuminant A, both with the same illuminance (100 cd/m^{-2}). Both figures show that the absorbed energy is much higher with standard illuminants than when lit by the system developed here.

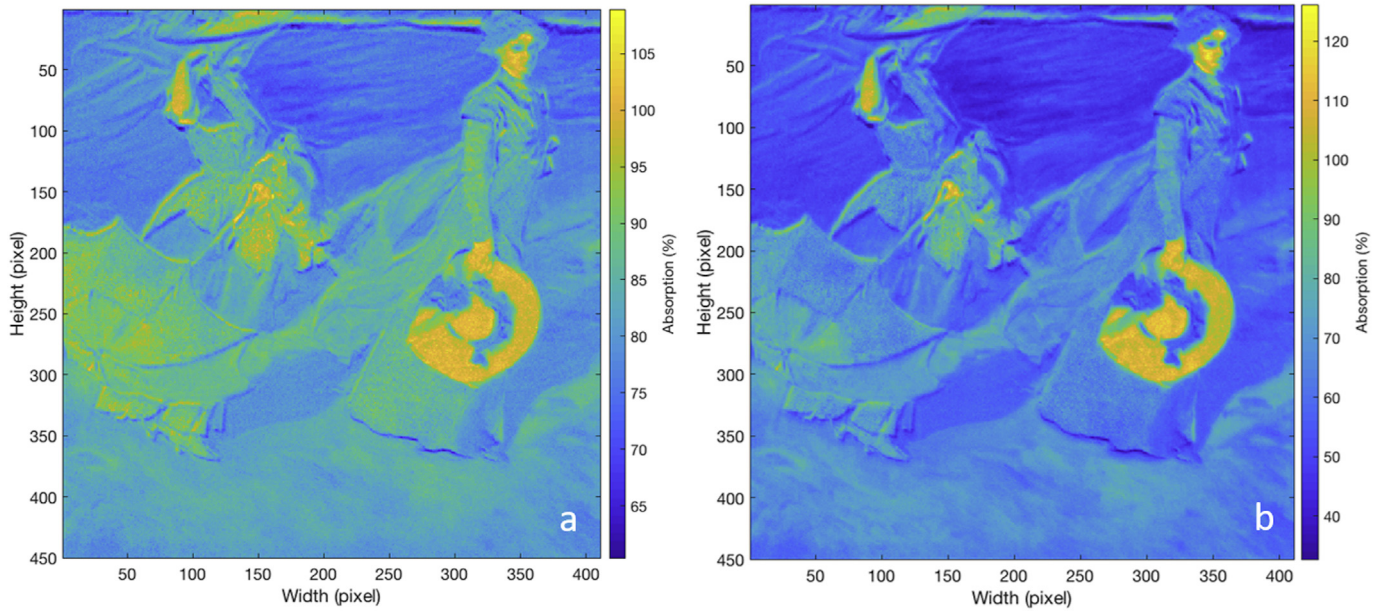

Fig. 13. Relative light absorption. (a) The amount of light absorbed by each pixel of the printed copy picture $\delta_{relative\ (x,y)}$ ranged from 61% to 109% under optimized lighting conditions, compared to the reference D65 illuminant. (b) The amount of light absorbed by each pixel ranged from 33% to 126% compared to the reference incandescent illuminant.

the non-damaged multi-colored painting under the reference daylight illuminant and the artificially damaged picture under optimized lighting conditions were imperceptible ($\Delta E_{00\_PK} = 0.27$), where $\Delta E_{00} = 1$ is a just-noticeable difference (JND) under controlled laboratory conditions. The amount of light absorbed by the painting, which could cause damage, was also reduced up to 40% compared to a daylight illuminant and reduced up to 67% when compared by an incandescent lamp.

These results show that a point-by-point optimized light projection system can substantially reduce damage to artwork and a decrease in energy consumption. Although the optimization algorithm minimizes the damage using the damage factor, it can be estimated that the light absorbed by the image of the printed copy, according to the reference studies, continues to cause damage. Absorption-minimizing light projection systems can offer a breakthrough in artwork conservation by preserving and virtually restoring artwork non-invasively.

Funding source

This research was supported by project RTI2018-097633-A-I00 from the Spanish Ministry funding "*Proyectos I + D Retos de Investigación*" entitled Photonic restoration applied to cultural heritage: application to Dali's picture "Dos Figuras".

Research data

Supplementary material associated with this article can be found, in the online version, at https://doi.org/10.17632/n8wzw5fpnx.1.

Appendix A. Supplementary data

Supplementary data to this article can be found online at https://doi.org/10.1016/j.daach.2019.e00128.

References

Al-Sallal, K.A., AbouElhamd, A.R., Dalmouk, M.B., 2018. UAE heritage buildings converted into museums: evaluation of daylighting effectiveness and potential risks on artifacts and visual comfort. Energy Build. 176, 333–359.

Bay, H., Ess, A., Tuytelaars, T., Van Gool, L., 2008. Speeded-up robust features (SURF). Comput. Vis. Image Understand. 110 (3), 346–359.

Berns, R.S., 2011. Designing white-light LED lighting for the display of art: a feasibility study. Color Res. Appl. 36 (5), 324–334.

Berns, R.S., 2019. Digital color reconstructions of cultural heritage using color-managed imaging and small-aperture spectrophotometry. Color Res. Appl. 16.

Bouguet, J., 2012. Camera calibration toolbox for Matlab. Comput. vis. Calif. Inst. Technol. http://www.vision.caltech.edu/bouguetj/calib_doc/.

Capel, D., Zisserman, A., 2003. Computer vision applied to super resolution. IEEE Signal Process. Mag. 20 (3), 75–86.

Chane, C.S., Mansouri, A., Marzani, F.S., Boochs, F., 2013. Integration of 3D and multispectral data for cultural heritage applications: survey and perspectives. Image Vis Comput. 31 (1), 91–102.

CIE, 2004a. 157:2004 Control of Damage to Museum Objects by Optical Radiation. CIE Commission Internationale de L'Eclairage Technical Report, p. 35.

CIE, 2004b. CIE 15:2004 Colorimetry.

Cuttle, C., 1996. Damage to museum objects due to light exposure. Light. Res. Technol. 28 (1), 1–9.

de Luna, J.M., Molini, D.V., Fernandez-Balbuena, A.A., Botella, A.G., Herraez, J.A., Ontañon, R., 2015. Selective spectral LED lighting system Applied in paleolithic cave art. Leukos 11 (4), 223–230.

De-Graaf, T., Mennatalla, D., Helmut, M.l., 2013. Sustainable lighting of museum buildings. Renew. Energy 0 (–).

Delgado, M.F., Dirk, C.W., Druzik, J., WestFall, N., 2011. Lighting the world's treasures: approaches to safer museum lighting. Color Res. Appl. 36 (4), 238–254.

Durmus, D., Davis, W., 2015a. Absorption-minimizing spectral power distributions. In: Light, Energy and the Environment 2015. Optical Society of America, Suzhou.

Durmus, D., Davis, W., 2015b. Optimising light source spectrum for object reflectance. Opt. Express 23 (11), A456–A464.

Durmus, D., Davis, W., 2017. Object color naturalness and attractiveness with spectrally optimized illumination. Opt. Express 25 (11), 12839–12850.

Durmus, D., Abdalla, D., Duis, A., Davis, W., 2018. Spectral optimization to minimize light absorbed by artwork. Leukos 1–10.

Fairchild, M.D., 2013. Color Appearance Models. John Wiley & Sons, Chichester, West Sussex, England.

Fechner, G.T., 1860. Elemente der Psychophysik (Leipzig: Breitkopf & Ha «rtel). In: *English translation of Vol. 1 by HE Adler 1966*. Holt, Rinehart, and Winston Inc, New York, NY.

Fernandez-Balbuena, A.A., Gonzalez, M., Garcia-Botella, A., Vazquez-Molini, D., 2015. Application of dynamic merit function to nonimaging systems optimization. Opt. Eng. 54 (2), 025107.

Hecht, J., 2015. Light repairs art: optical overlays restore faded masterworks. Opt. Photonics News 26 (4), 40–47.

Hilbert, G., Aydinli, S., Krochmann, J., 1991. Zur beleuchtung musealer exponate: neuere konservatorische erkenntnisse. Restauro 97 (5), 313–321.

Hunt, R.W.G., 1952. Light and dark adaptation and the perception of color. JOSA 42 (3), 190–199.

Hwang, S., Song, H., Cho, S.-W., Kim, C.E., Kim, C.-S., Kim, K., 2017. Optical measurements of paintings and the creation of an artwork database for authenticity. PLoS One 12 (2), 1–14.

Imai, F.H., Rosen, M.R., Berns, R.S., 2000. Comparison of spectrally narrow-band capture versus wide-band with a priori sample analysis for spectral reflectance estimation. In: Color and Imaging Conference. Society for Imaging Science and Technology.

Lagarias, J.C., Reeds, J.A., Wright, M.H., Wright, P.E., 1998. Convergence properties of the nelder–mead simplex method in low dimensions. SIAM J. Optim. 9 (1), 112–147.

Lin, W.C., Huang, T.S., Ho, T.C., Chen, Y.T., Chuang, J.H., 2013. Interactive lighting design with hierarchical light representation. Comput. Graph. Forum 32 (4), 133–142 (Wiley Online Library).

Marimont, D.H., Wandell, B.A., 1992. Linear models of surface and illuminant spectra. J. Opt. Soc. Am. A 9 (11), 1905–1913.

Mayorga, S., Vazquez, D., Fernandez-Balbuena, A.A., Hernandez, G., Herraez, J.A., Azcutia, M., Garcia, A., 2016a. Advanced daylighting evaluation applied to cultural heritage buildings and museums: application to the cloister of Santa Maria El Paular. Renew. Energy 85, 1362–1370.

Mayorga, S., Vazquez, D., Fernandez-Balbuena, A.A., Muro, C., Muñoz, J., 2016b. Spectral damage model for lighted museum paintings: oil, acrylic and gouache. J. Cult. Herit. 22, 931–939.

Michalski, S., 2013. Agent of Deterioration: Light, Ultraviolet and Infrared. Canadian Conservation Institute, Ottawa. Last modified **6**.

Miller, J.V., 1993. Evaluating Fading Characteristics of Light Sources. NoUVIR Research.

Mueller, H.F., 2013. Energy efficient museum buildings. Renew. Energy 49, 232–236.

Murakami, Y., Yamaguchi, M., Ohyama, N., 2012. Hybrid-resolution multispectral imaging using color filter array. Opt. Express 20 (7), 7173–7183.

Nelder, J., Mead, R., 1965. A simplex method for function minimization. Comput. J. 7 (4), 6.

Pavlogeorgatos, G., 2003. Environmental parameters in museums. Build. Environ. 38, 1457–1462.

Perrin, T., Druzik, J., Miller, N., 2014. SSL Adoption by Museums: Survey Results, Analysis, and Recommendations. Pacific Northwest National Lab.(PNNL), Richland, WA (United States).

Phillips, D.C., 1912. Sorolla: the painter of sunlight. Art Prog. 791–797.

Pridmore, R.W., 1999. Bezold–Brucke hue-shift as functions of luminance level, luminance ratio, interstimulus interval and adapting white for aperture and object colors. Vis. Res. 39 (23), 3873–3891.

Quiroga, J.A., Zoido, J., Alonso, J., Bernabeu, E., 1994. Colorimetric matching by minimum-square-error fitting. App. Opt. Opt. Soc. Americ 33 (26), 3.

Saunders, D., Kirby, J., 1994. Wavelength-dependent Fading of Artists' Pigments, pp. 190–194.

Schaeffer, T.T., 2002. Effects of Light on Materials in Collections: Data on Photoflash and Related Sources. Getty Publications, Los Angeles.

Schanda, J., 2007. Colorimetry. Understanding CIE System. John Wiley & Sons.

Sharma, G., Wu, W., Dalal, E.N., 2005. The CIEDE2000 color-difference formula: implementation notes, supplementary test data, and mathematical observations. Color Res. App. 30 (1), 21–30.

Shen, H.L., Cai, P.Q., Shao, S.J., Xin, J.H., 2007. Reflectance reconstruction for multispectral imaging by adaptive Wiener estimation. Optics express 15 (23), 15545–15554.

Simpson, M.L., Jansen, J.F., 1991. Imaging colorimetry: a new approach. Applied Optics 30 (32), 4666–4671.

Stenger, J., Khandekar, N., Raskar, R., Cuellar, S., Mohan, A., Gschwind, R., 2016. Conservation of a room: a treatment proposal for mark Rothko's harvard murals. Studies in Conservation 61 (6), 348–361.

Viénot, F., Coron, G., Lavédrine, B., 2011. LEDs as a tool to enhance faded colours of museums artefacts. J. Cult. Herit. 12 (4), 431–440.

Vincent, E., Laganière, R., 2005. Detecting and matching feature points. J. Vis. Commun. Image Represent. 16 (1), 38–54.

Zhang, Z., 2000. A flexible new technique for camera calibration. IEEE Trans. Pattern Anal. Mach. Intell. 22 (11), 1330–1334.

Update

Digital Applications in Archaeology and Cultural Heritage
Volume 24, Issue , March 2022, Page

DOI: https://doi.org/10.1016/j.daach.2021.e00209

Digital Applications in Archaeology and Cultural Heritage 24 (2022) e00209

Contents lists available at ScienceDirect

Digital Applications in Archaeology and Cultural Heritage

journal homepage: www.elsevier.com/locate/daach

Erratum regarding missing Declaration of Competing Interest statements in previously published articles – Part 1

Declaration of Competing Interest statements were not included in the published version of the following articles that appeared in previous issues of Digital Applications in Archaeology and Cultural Heritage.

The appropriate Declaration/Competing Interest statements, provided by the Authors, are included below.

1. "Stepping stones: Virtual restoration and 3D visualisation of the tessellated 4th century Byzantine synagogue floor at Apamea on Orontes, Syria" [Digital Applications in Archaeology and Cultural Heritage, 2019; 15: e00108] 10.1016/j.daach.2019.e00108

Declaration of competing interest: The author declares that they have no known competing financial interests or personal relationships that could have appeared to influence the work reported in this paper.

2. "Bringing a peripheral, traditional venue to the digital era with targeted narratives" [Digital Applications in Archaeology and Cultural Heritage, 2019; 14: e00111] 10.1016/j.daach.2019.e00111

Declaration of competing interest: The author declares that they have no known competing financial interests or personal relationships that could have appeared to influence the work reported in this paper.

3. "Emerging materiality through dynamic digital conservation" [Digital Applications in Archaeology and Cultural Heritage, 2021; 23: e00198] 10.1016/j.daach.2021.e00198

Declaration of competing interest: The author declares that they have no known competing financial interests or personal relationships that could have appeared to influence the work reported in this paper.

4. "Enhancing learning and access to Underwater Cultural Heritage through digital technologies: The case study of the "Cala Minnola" shipwreck site" [Digital Applications in Archaeology and Cultural Heritage, 2019; 13: e00103] 10.1016/j.daach.2019.e00103

Declaration of competing interest: The author declares that they have no known competing financial interests or personal relationships that could have appeared to influence the work reported in this paper.

5. "Energy optimization of a light projection system for buildings that virtually restores artworks" [Digital Applications in Archaeology and Cultural Heritage, 2019; 16: e00128] 10.1016/j.daach.2019.e00128

Declaration of competing interest: The author declares that they have no known competing financial interests or personal relationships that could have appeared to influence the work reported in this paper.

6. "A method for similarity assessment between death masks and portraits through linear projection: The case of Vincenzo Bellini" [Digital Applications in Archaeology and Cultural Heritage, 2020; 17: e00144] 10.1016/j.daach.2020.e00144

Declaration of competing interest: The author declares that they have no known competing financial interests or personal relationships that could have appeared to influence the work reported in this paper.

7. "Implementing a protocol for employing three-dimensional representations in archaeology (PETRA) for the documentation of neolithic funeral architecture in Western France" [Digital Applications in Archaeology and Cultural Heritage, 2019; 13: e00096] 10.1016/j.daach.2019.e00096

Declaration of competing interest: The author declares that they have no known competing financial interests or personal relationships that could have appeared to influence the work reported in this paper.

8. "Ancient machine tools for the construction of the Antikythera Mechanism parts" [Digital Applications in Archaeology and Cultural Heritage, 2019; 13: e00092] 10.1016/j.daach.2019.e00092

Declaration of competing interest: The author declares that they have no known competing financial interests or personal relationships that could have appeared to influence the work reported in this paper.

DOIs of original article: https://doi.org/10.1016/j.daach.2019.e00111, https://doi.org/10.1016/j.daach.2019.e00093, https://doi.org/10.1016/j.daach.2019.e00096, https://doi.org/10.1016/j.daach.2018.e00089, https://doi.org/10.1016/j.daach.2020.e00140, https://doi.org/10.1016/j.daach.2019.e00092, https://doi.org/10.1016/j.daach.2019.e00133, https://doi.org/10.1016/j.daach.2019.e00108, https://doi.org/10.1016/j.daach.2019.e00097, https://doi.org/10.1016/j.daach.2020.e00144, https://doi.org/10.1016/j.daach.2020.e00146, https://doi.org/10.1016/j.daach.2019.e00128, https://doi.org/10.1016/j.daach.2021.e00198, https://doi.org/10.1016/j.daach.2019.e00103, https://doi.org/10.1016/j.daach.2020.e00141.

https://doi.org/10.1016/j.daach.2021.e00209

Available online 22 December 2021

9. “Heritage documentation using laser scanner and photogrammetry. The case study of Qasr Al-Abidit, Jordan” [Digital Applications in Archaeology and Cultural Heritage, 2019; 16: e00133] 10.1016/j.daach.2019.e00133

Declaration of competing interest: The author declares that they have no known competing financial interests or personal relationships that could have appeared to influence the work reported in this paper.

10. “Digital workflow to improve osteoarchaeological documentation” [Digital Applications in Archaeology and Cultural Heritage, 2019; 13: e00097] 10.1016/j.daach.2019.e00097

Declaration of competing interest: The author declares that they have no known competing financial interests or personal relationships that could have appeared to influence the work reported in this paper.

11. “Knowledge-based model for geomaterials in the Ancient Centre of Naples (Italy): Towards an integrated approach to cultural heritage” [Digital Applications in Archaeology and Cultural Heritage, 2020; 18: e00146] 10.1016/j.daach.2020.e00146

Declaration of competing interest: The author declares that they have no known competing financial interests or personal relationships that could have appeared to influence the work reported in this paper.

12. “Lost colours: Photogrammetry, image analysis using the DStretch plugin, and 3-D modelling of post-firing painted pottery from the south west Iberian Peninsula” [Digital Applications in Archaeology and Cultural Heritage, 2019; 13: e00093] 10.1016/j.daach.2019.e00093

Declaration of competing interest: The author declares that they have no known competing financial interests or personal relationships that could have appeared to influence the work reported in this paper.

13. “Antikythera mechanism – A compound epicyclic gearing for Venus” [Digital Applications in Archaeology and Cultural Heritage, 2019; 12: e00089] 10.1016/j.daach.2018.e00089

Declaration of competing interest: The author declares that they have no known competing financial interests or personal relationships that could have appeared to influence the work reported in this paper.

14. “Efficient three-dimensional field documentation methods for labour cost studies: Case studies from archaeological and heritage contexts” [Digital Applications in Archaeology and Cultural Heritage, 2020; 17: e00141] 10.1016/j.daach.2020.e00141

Declaration of competing interest: The author declares that they have no known competing financial interests or personal relationships that could have appeared to influence the work reported in this paper.

15. “Distant augmented reality: Bringing a new dimension to user experience using drones” [Digital Applications in Archaeology and Cultural Heritage, 2020; 17: e00140] 10.1016/j.daach.2020.e00140

Declaration of competing interest: The author declares that they have no known competing financial interests or personal relationships that could have appeared to influence the work reported in this paper.